



Hot electron emission characteristics from thin metal foil targets irradiated by terawatt laser

Research Article



Cite this article: Singh S *et al.* (2024) Hot electron emission characteristics from thin metal foil targets irradiated by terawatt laser. *Laser and Particle Beams* **42**, e2, 1–9. <https://doi.org/10.1017/lpb.2023.2>

Received: 3 November 2023
Accepted: 24 November 2023

Keywords:

electron temperature scaling; hot electron generation; inertial fusion; laser-foil interaction; multi-channel electron spectrometers; plasma physics

Corresponding authors: Sushil K. Singh;
Email: singh@ipp.cas.cz;
M. Krupka;
Email: krupka@pals.cas.cz

Sushil K. Singh^{1,2,3} , Michal Krupka^{1,2,3,4} , Josef Krasa¹, Valeria Istokskaia^{4,5}, Jan Dostal^{1,2}, Roman Dudzak^{1,2}, Tadeusz Pisarczyk⁶, Jakub Cikhardt³, Shubham Agarwal^{2,7}, Daniel Klir³, Karel Rezac³, Lorenzo Giuffrida⁵, Tomasz Chodukowski⁶, Zofia Rusiniak⁶, Tomas Burian^{1,2}, Daniele Margarone^{5,8}, Miroslav Krus¹ and Libor Juha²

¹Laser-Plasma Department, Institute of Plasma Physics, Czech Academy of Sciences, Prague, Czech Republic; ²Department of Radiation and Chemical Physics, FZU – Institute of Physics, Czech Academy of Sciences, Prague, Czech Republic; ³Department of Physics, Faculty of Electrical Engineering, Czech Technical University in Prague, Czech Republic; ⁴Department of Physical Electronics, Faculty of Nuclear Sciences and Physical Engineering, Czech Technical University in Prague, Prague, Czech Republic; ⁵ELI Beamlines, The Extreme Light Infrastructure ERIC, Dolni Brezany, Czech Republic; ⁶Department of Laser Plasma and Applications, Institute of Plasma Physics and Laser Microfusion, Warsaw, Poland; ⁷Department of Surface and Plasma Physics, Faculty of Mathematics and Physics, Charles University, Czech Republic and ⁸Centre for Light-Matter Interactions, School of Mathematics and Physics, Queen's University Belfast, Belfast, UK

Abstract

The interaction of focused high power laser beam with solid targets leads to acceleration of charged particles among other by non-linear effects in the plasma. In this experiment, the hot electrons are characterized from the interaction of sub-nanosecond and kilo-joule class laser pulse with thin metal foil targets (Cu, Ta, Ti, Sn, Pb). The energy distribution functions of electrons were measured by angularly resolved multichannel electron spectrometer. The hot electron temperatures were observed in range from 30 to 80 keV for laser intensities between $\sim 10^{15}$ and 3×10^{16} W cm⁻². The measured energy distribution and electron temperature were compared with published results and known scaling laws at higher laser intensities. For foil targets of different materials, the temperature and flux of hot electrons were scaled with target thickness in the range of 1–100 μ m from low Z to high Z materials where Z is the atomic number. The profile of conversion efficiency from laser energy to hot electrons is discussed in the energy range from 100 to 600 J. For the given laser and target parameters, the nonlinear behaviour of conversion efficiency and relevant physics are also described in detail.

Introduction

The interaction of laser radiation with solid matter at intensities above 10^{15} W cm⁻² gives rise to the ionization of matter, creating plasma on the surface of the target, and leads to production of accelerated particles and X-ray photons (Refs 1, 2). In the recent years, high-energy and high-intensity laser-plasma experiments have been used to study the generation of energetic particles and high energy radiation (Ref. 3). The production of hot electron in laser-plasma interaction (LPI) has important relevance not only in the context of inertial confinement fusion (Refs 4, 5) but also broadens the understanding of the generation mechanism of spontaneous magnetic field (Refs 6, 7) as well as experimental studies in high-energy density physics (Ref. 8) and laboratory astrophysics (Ref. 9).

When a high intensity laser pulse interacts with a solid target, its prepulse having duration up to several nanoseconds and intensity level $\sim 10\%$ of the maximum amplitude, creates a preplasma. The interaction of the main laser pulse with this preplasma produces relativistic electrons (Ref. 3) by various physical processes, such as resonance absorption (Ref. 10), vacuum heating (Ref. 11), betatron resonance (Ref. 12), wakefield acceleration (Refs 13, 14), inverse bremsstrahlung, etc. (Refs 15, 16). One of the important aspects governing these processes is laser absorption into hot electrons (Ref. 17). These electrons subsequently penetrate inside the target and produce bremsstrahlung emission (Ref. 17), which constitutes an X-ray source that may be used in various applications, such as radiography of dense plasma (Ref. 18), photonuclear studies (Refs 19, 20). Moreover, the collisional effect is found to be significant when the incident laser intensity is less than 10^{16} W cm⁻² (Ref. 21), which tends to enhance the resonance absorption and reduce the vacuum heating under different plasma parameters. At higher intensities, various collisionless absorption mechanisms dominate with a large number of hot

© The Author(s) 2024. Published by Cambridge University Press. This is an Open Access article, distributed under the terms of the Creative Commons Attribution licence (<http://creativecommons.org/licenses/by/4.0/>), which permits unrestricted re-use, distribution and reproduction, provided the original article is properly cited.

electrons produced. The scaling of hot electron temperatures is found to depend upon the dominant absorption mechanisms (Ref. 21). The precise measurements of the energy distribution and temperature of hot electrons at different laser intensity are crucial for better understanding of these mechanisms.

The multichannel electron spectrometers based on magnetic deflection (Ref. 22) have often been used to provide an indication on the angular distribution of fast electrons escaped from the target plasma. Moreover, indirect measurements of bremsstrahlung radiation generated by such hot electrons inside the plasma provides the quantitative estimate of the fast electron energy distribution, conversion efficiency of laser energy into fast electrons and their angular distribution (Refs 23, 24). The intense emission of hot electrons in laser–solid interaction depends on achieving the highest possible conversion efficiency and electron temperature with the least amount of invested laser energy. The conversion efficiency of laser energy into electron energy and associated bremsstrahlung radiation relies on the laser energy, intensity, material, geometry and thickness of the target (Ref. 25). In the recent experiment, Rusby *et al.* reported results from a high-intensity and picosecond scale laser interaction with cone targets that significantly increase the temperature and flux of the hot electrons over a traditional planar target (Ref. 26). The enhancement in electron temperature and flux is caused by a substantial increase in the plasma density within the cone target geometry, which was induced by a prepulse that arrived 1.5 ns prior to the main laser intensity ($\geq 10^{19}$ W cm⁻²).

Since very limited investigations have been reported on the characterization of the hot electrons produced by kJ-ns class lasers, in this experiment carried out at the Prague Asterix Laser System (PALS) (Ref. 27), hot electrons are characterized by interaction of sub-nanosecond laser beam with thin metal foil targets (Cu, Ta, Ti, Sn, Pb) for laser intensities between 4×10^{15} and 3×10^{16} W cm⁻². The thicknesses of the foil targets were varied for optimizing the emitted electron temperature and energy distribution in angular direction with laser axis. The energy distribution functions of electrons were measured by angularly resolved multichannel electron spectrometer (Ref. 22). The energy distribution and electron temperature were compared with experimental and simulation results and known scaling laws at higher laser intensities. In addition, the angular characteristics of hot electrons spectra are scaled with laser energy and target thickness of different materials. Due to the nanosecond duration of the laser pulse at the 10% level of the laser pulse maximum, the peak of laser pulse interacts with the preplasma produced by front of the laser pulse also plays an important role in generation of hot electrons. Moreover, in non-relativistic

regime the conversion efficiency of hot electron energy from laser energy is also discussed for different target materials. For the given experimental conditions, nonlinearity associated in the profile of conversion efficiency and relevant physics are also summarized.

The paper is organized as follows. The experimental layout and diagnostic system are described in ‘Experimental layout and diagnostic system’ section. The description of the experimental results is discussed in ‘Experimental results’ section. The major outcome and summary of the paper are presented in next section. The conclusion is summarized in last section.

Experimental layout and diagnostic system

The experiment was carried out at the PALS facility using a single beam iodine photodissociation laser system (Ref. 27). The layout of the experimental set-up is shown in Figure 1. The iodine laser supplies up to 700 J of energy at the fundamental wavelength 1.315 μ m with pulse duration ≈ 350 ps. The laser is capable to deliver the energy up to 700 J onto a target. The laser beam is focused to a spot of diameter ≈ 100 μ m using a $f/2$ aspherical lens with focal length 600 mm, reaching the power density up to 3×10^{16} W cm⁻². The repetition rate of the laser system is one shot per 30 min and the polarization of the output beam is linear. The focused beam was incident on targets at normal incidence in the equatorial plane. The intensity of the laser pulse was varied in the range of 4×10^{15} to 3×10^{16} W cm⁻². The targets were chosen from different materials (low to high Z, where Z is the atomic number of the material), such as Ti, Cu, Sn, Ta and Pb foils. The thickness of foil targets were ranges between 1 and 100 μ m. The metal foils were irradiated by laser pulse in the energy range between 100 and 600 Joules.

The angularly resolved multichannel magnetic electron spectrometers were developed for the measurements of the energy distribution of hot electrons (Ref. 22). The spectrometers were installed in an angular array configuration around the foil target covering the angles on the horizontal plane as shown in Figure 1. The compact design, innovative idea of the plastic collimator and shielding mechanism were implemented in the geometry of the spectrometers to reduce the background noise from the measurements. The aperture (≈ 1 mm) of each spectrometer subtended a solid angle of about $\approx 10^{-5}$ sr at the target centre. The collimated electrons are spectrally dispersed in a magnetic field and detected by an image plate (IP) of type BAS-Super Resolution (BAS-SR). The IPs were absolutely calibrated to provide absolute electron flux for respective electron energies (Ref. 28). The spectrometer measures

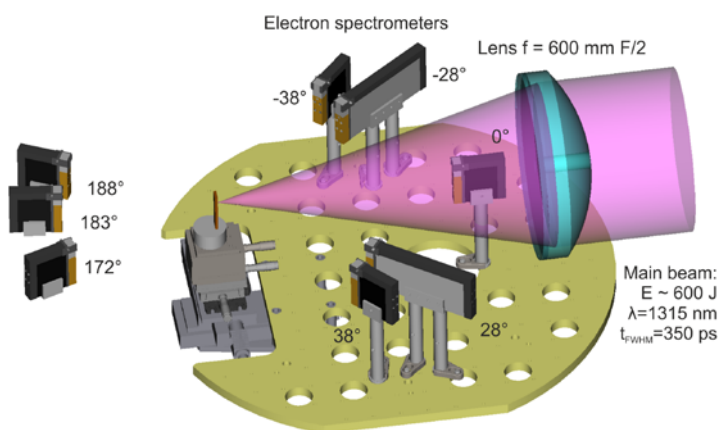


Figure 1. The typical layout of the experimental setup along with angularly resolved multichannel electron spectrometer. In this configuration, eight electron spectrometers are placed at various angles from the direction of laser beam. The spectrometers are installed at the breadboard inside a vacuum chamber.

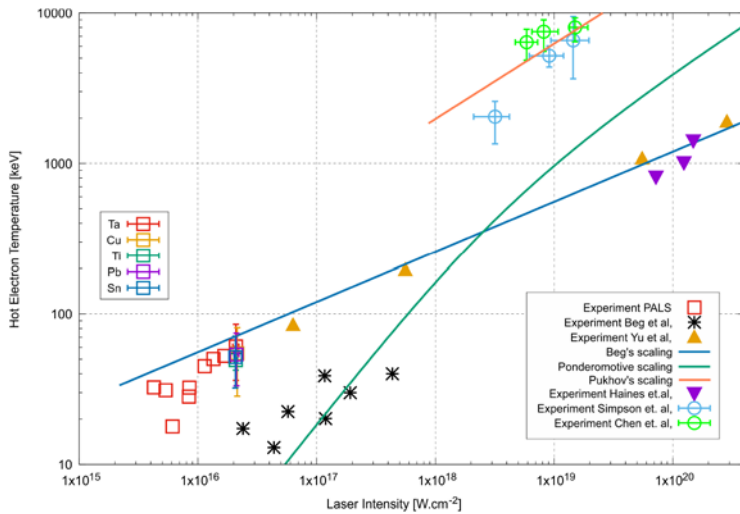


Figure 2. The variation of hot electron temperature as function of laser intensity for different target materials (Ta, Cu, Ti, Pb & Sn) having similar thickness range, i.e. $\approx 10 \mu\text{m}$ (see square symbols). The electron temperature scaling is compared with known Beg (Ref. 29), ponderomotive (Ref. 30) and Pukhov (Ref. 31) scaling laws. These measurements are also scaled from the experiments of sub-nanosecond, sub-picosecond and multi-picosecond laser-matter interaction at different laser facilities. The legend symbols correspond to specific targets and references relevant with data for the temperature scaling (Refs 24, 29–36).

electron energies in the range from 50 keV to 2.5 MeV using ferrite magnets having magnetic field of 95 mT (Ref. 22).

Experimental results

In this experiment, we have characterized physical quantities derived from the hot electron energy distribution functions measured by an array of electron spectrometers. By means of experimental observations, we determined hot electron temperature, total number of emitted electrons, charge, maximum electron energy and the conversion efficiency from laser energy to hot electrons.

Figure 2 shows the temperature scaling of hot electron with laser intensity for different target materials, such as Ta, Cu, Ti, Pb and Sn. For PALS laser and plasma parameters, electron temperature (T_{hot}) varies in the range from 20 to 80 keV in the intensity range from 4×10^{15} to $3 \times 10^{16} \text{ W cm}^{-2}$. In addition, the temperature scaling of different targets is compared with experimental and simulation results from sub-nanosecond, sub-picosecond and multi-picosecond laser systems (see Figure 2 and relevant references) (Refs 24, 29–35). The electron temperature T_{hot} is considerably higher than the ‘suprathermal’ temperature, which should be less than 20 keV in our experiment (Refs 37, 38). The electron temperature from measured data shows that the temperature scaling is mostly consistent with the Beg scaling (Ref. 29), i.e. $T_{\text{hot}} \approx (I\lambda^2)^{1/3}$, where I and λ are the laser intensity and wavelength, respectively. The Beg scaling is typically observed for picosecond laser-matter interaction which is in agreement with the experimental results by Kluge et al. (Ref. 39). Moreover, past experimental results by Kluge et al. (Ref. 34) show that at lower laser intensities ($\leq 10^{16} \text{ W cm}^{-2}$), the electron temperature scaling varies in between Beg scaling and ponderomotive scaling (see Eqn. 1) (Ref. 30) which are also in closer agreement with results shown in Figure 2:

$$T_{\text{hot}} = 511 \left(\sqrt{1 + \frac{I \lambda^2 [\text{W cm}^{-2} \mu\text{m}^2]}{1.37 \times 10^{18}}} - 1 \right) [\text{keV}]. \quad (1)$$

Furthermore in the under-dense region of the plasma, primarily produced via ablation from the laser prepulse, electron acceleration

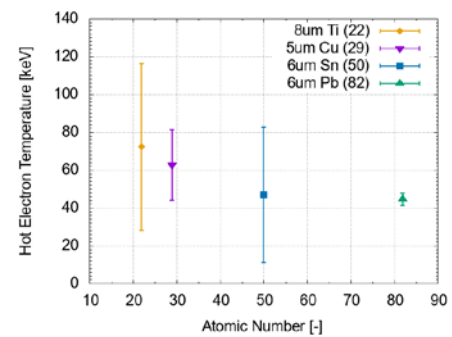


Figure 3. Dependence of hot electron temperature with respect to target material for the very thin foil targets (thickness range: 5–8 μm). The errorbar associated with each data point represents shot to shot fluctuation.

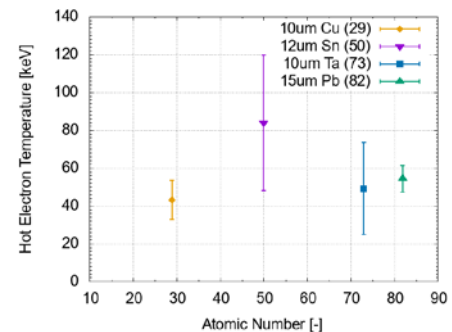


Figure 4. Dependence of hot electron temperature with respect to target material for the moderately thin foil targets, i.e. thickness range: 10–15 μm .

occurs due to stochastic processes. It should be noted that for relatively high laser intensity $\geq 10^{18} \text{ W cm}^{-2}$, the electron temperature is given by Pukhov scaling (Ref. 31), i.e. $T_{\text{hot}} \approx 1.5 \times \sqrt{(I\lambda^2/10^{18})}$ [MeV]. In high intensity and multi-picosecond laser-plasma experiments, the measured electron temperature by Chen et al. (Ref. 35) and Simpson et al. (Ref. 36) were found in close agreement with Pukhov scaling as shown in Figure 2.

The hot electron temperature T_{hot} is determined by the slope of the energy distribution measured T_{hot} using multichannel electron

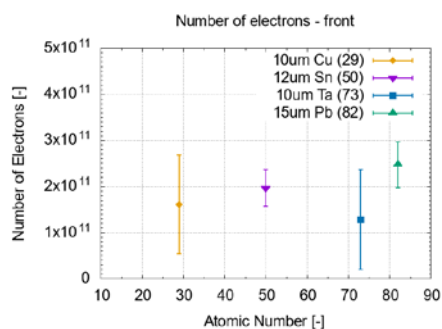


Figure 5. The variation in total number of hot electrons in the front side of the target with respect to laser direction for elements with increasing atomic number.

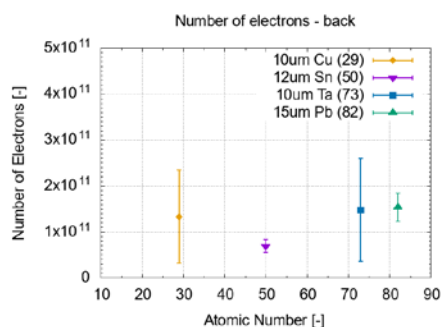


Figure 6. The profile of hot electron flux in the back side of the target for the same elements (low to high Z) as shown in Figure 5.

spectrometer. Figures 3 and 4 show the hot electron temperature as function of different atomic numbers for thin (5–8 μm) and relatively thick foil (10–15 μm) targets, respectively. The target thickness of individual metal foil is mentioned in Figures 3 and 4. The electron temperature varies in the range from 30 to 80 keV for respective foil targets. For thin foil targets, the electron temperature is slowly decreasing with increasing atomic numbers however, it does not depend on atomic numbers for relatively thick foil targets (see Figure 4).

The total flux of hot electrons was measured by spectrometers in the front and back directions with respect to target plane and laser axis. Figures 5 and 6 show the total number of hot electrons emitted from the foil targets having different Z in front and back direction, respectively. The results indicate that in front direction from foil targets, the total electron flux increases slightly with increasing atomic numbers (Z) however, it does not strongly depend on atomic numbers in the back directions (see Figure 6). The different characteristics of electron flux in front and backward directions could be attributed to the recirculation and scattering of electrons inside the target plasma. In addition, it is noted that the optical thickness of the target is also important in the hot electron characteristics which is described later in this section. Moreover, due to the Z-dependence of the conversion from laser energy to hot electrons, the appropriate target consist of a high Z material is recommended for the experiment to increase hot electron flux.

In the laser-target interaction experiment, the characteristics of the plasma and emitted electrons also depend on the thickness of the target material. Figure 7 shows the variation in electron temperature for the different thickness (1–100 μm) of the copper target for similar laser energy in the range of 550 and 600 J. The electron temperature varies in the range between 30 and 90 keV;

however, the average electron temperature is around 50 keV. The electron temperature is relatively high (≥ 60 keV) for thin targets (2–5 μm) and it is comparatively lower (≤ 40 keV) for the thick targets (≥ 10 μm). In the case of thick targets, lower temperature of hot electrons can be attributed to recirculation, refluxing or scattering of electrons inside the target plasma (Ref. 40).

Figures 8 and 9 represent the variation of electron flux with target thickness for copper target in front and back directions, respectively, for the same laser energy as discussed in Figure 7. The profiles of Figs. 8 and 9 show that electron flux is higher for thin target (≤ 10 μm) and flux decreases as target thickness increases in both front and back direction. The deficiency in electron flux can be attributed to expected energy lost by hot electrons while traversing thick targets (Ref. 41). The results conclude that for the given laser parameters, thin targets are appropriate choice for optimal generation of hot electrons.

In order to characterize the hot electron emission, measurements relevant with angular distribution of electron energy are essential. Figure 10 represents the angular characteristics of hot electron temperature and electron flux at different angles with laser axis for 10 μm thick copper and tantalum targets, respectively. The results indicate that the hot electron temperature is in the range of 40–60 keV (see Figure 10(A)) and it depends on angular direction for both target materials, i.e. the electron temperature is bit higher at laser axis in comparison with other angular directions. Following the profile of electron temperature, electron flux shows similar characteristics (see Figure 10(B)). The flux is higher along the laser axis and it decreases along angular directions for both kind of targets. However, it should be noted that hot electron temperature and flux is slightly higher in case of 10 μm thick tantalum target in comparison to copper target having same thickness. Comparatively higher electron flux for tantalum case is attributed to high Z material which has been used as a bremsstrahlung converter for better efficiency in high intensity laser–solid interaction experiments (Ref. 25).

Total conversion efficiency associated with laser energy to hot electron is also determined for mentioned targets having different materials. In this case, the thickness of all targets was kept within a similar range, i.e. of the order of 10 μm . Total number of hot electrons per shot ($\sim 6 \times 10^{11}$) is estimated by integrating the measured electron spectra in angular direction to the entire 4π solid angle which corresponds to total charge of about ~ 0.1 μC . The total energy carried with these electrons is of the order of 6 mJ. This implies a conversion efficiency from laser energy (~ 600 J) to electrons of about $\sim 0.001\%$. In addition, the measured profile of the conversion efficiency associated with specific targets for different laser energy is shown in Figure 11. The characteristics of the profile show step-like behaviour in the laser energy above 200 J. We observed that conversion efficiency is varying nonlinearly with increasing laser energy in the range between $\sim 10^{-6}$ and $\sim 10^{-3}$ for laser energy from 100 to 600 J (Ref. 24). The physical mechanism relevant with these nonlinearities is described in the next section.

Summary and discussion

The paper outlined the results of temperature scaling and characteristics of hot electrons from thin foil metal targets irradiated by terawatt class iodine laser. It has already been reported that laser-plasma instabilities and relevant nonlinear processes due to spacial inhomogeneities in plasma density and electron temperature play a major role in the fluctuations of the plasma parameters (Ref. 42). Laser energy deposited near plasma critical density is

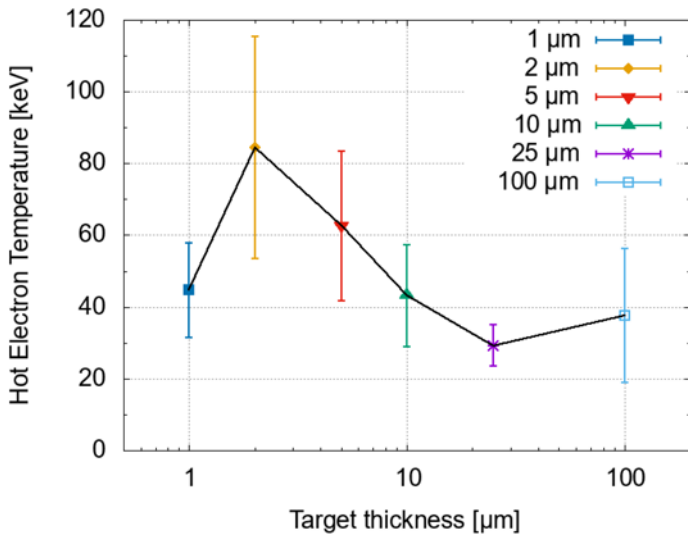


Figure 7. Dependence of hot electron temperature with respect to the thickness of the copper target. The result indicates that electron temperature decreases with increasing target thickness.

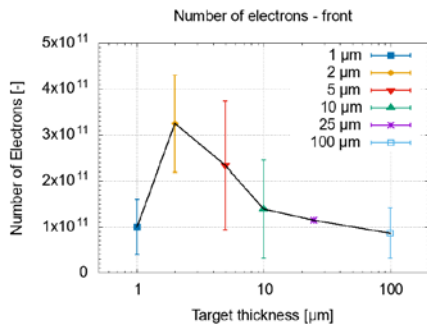


Figure 8. Number of emitted electrons from the front side with respect to the different thickness of copper target.

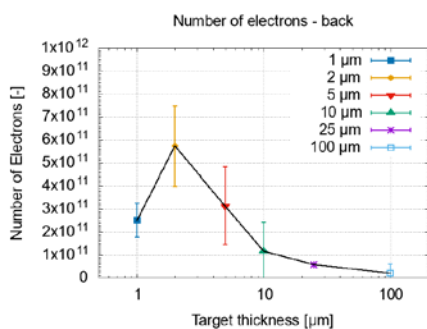


Figure 9. Number of emitted electrons from the back side with respect to the different thickness of copper target.

thermally transported to denser and cooler regions, causing more material ablation, creating inward directed ablation pressure, as well as producing X-rays (bremsstrahlung radiation) in the target. As shown in Figures 3–10, ablation depends on the characteristics of the target material, i.e. atomic number and its thickness. The largest fluctuations of the electron temperature are observed in Ti and Sn plasmas, however, fluctuations in number density of fast electrons can be found in the Ta and Cu plasmas. It should be noted that plasma produced using Sn targets show very low density fluctuations which is in contrary to relatively high temperature

fluctuations for the same target parameters. On the other hand, Pb plasma shows low fluctuations in density as well as in electron temperature measurements. In physical mechanism, the ponderomotive force that drives plasma density and temperature fluctuations depends on the spatial gradient of the electric field pressure due to the beating between the laser and scattered light waves driven by parametric instabilities, such as stimulated Raman scattering (SRS) and two-plasmon decay (TPD) (Ref. 43). In the case of parametric instabilities, the convective growth of the scattered light is the thermal noise which arises from Thomson scattering of the thermal density fluctuations as well as bremsstrahlung from the hot plasma. In addition to the parametric instabilities, self-focusing of the laser light can also play a crucial role in the fluctuations, causing the laser beam to filament and increase its intensity. Self-focusing occurs due to localized intense region of the laser which creates a plasma density depression, in presence of laser driven ponderomotive pressure or localized thermal heating. The density depression acts like a positive lens, further focusing the intense region, creating an unstable situation. Since self-focusing increases the laser intensity, this can further lead to increased growth rate of parametric instabilities. A counter interplay between these processes enhances the shot-shot fluctuations in the plasma parameters. Moreover, the hydrodynamic evolution of the target also affected the levels of parametric instabilities due to density and velocity fluctuations from the plasma formation process. Furthermore, quasi-spherical nature of the ablative expansion of the plasma and associated density distribution can be related to diverse mechanisms including relevant plasma instabilities, spontaneous magnetic field pressure gradient and partially also a nonideality of the irradiation process (Ref. 23). In order to avoid shot to shot fluctuations in the laser-plasma experiments, single shot can be recommended for the precise measurements and cross verification with additional supporting diagnostics however, single shot measurement is limited by the statistical uncertainty in the measured data.

As shown by Figure 2, electron temperature scaling is compared by Beg, ponderomotive and Pukhov scalings along with other experimental results obtained using sub-nanosecond, sub-picosecond and multi-picosecond lasers. In this experiment, the measured data points are consistent with the fact that at lower laser intensities ($\leq 10^{16} \text{ W cm}^{-2}$), the electron temperature scaling

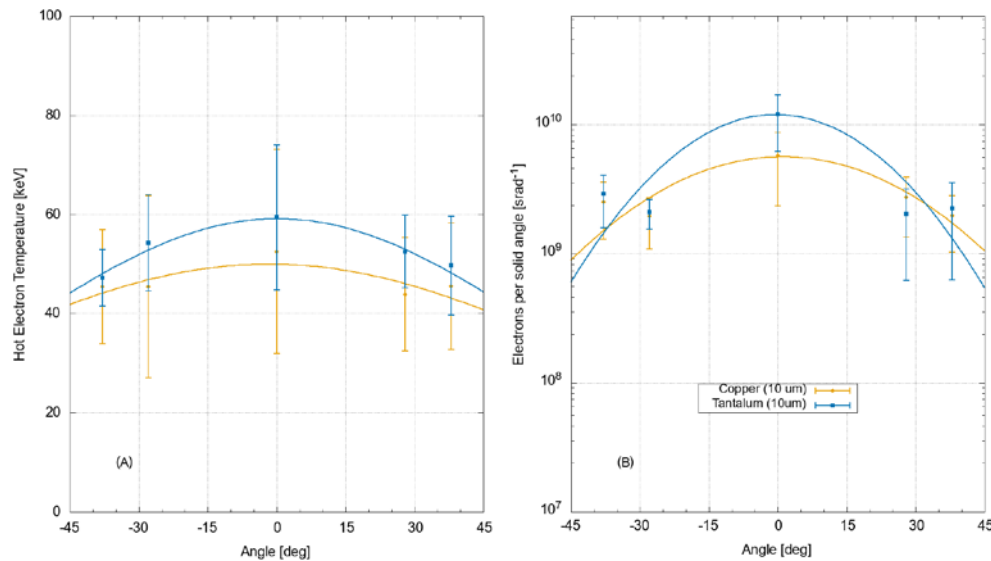


Figure 10. A comparison of angular characteristics of hot electron temperature (A) and flux (B) in between copper and tantalum targets (see legend colours).

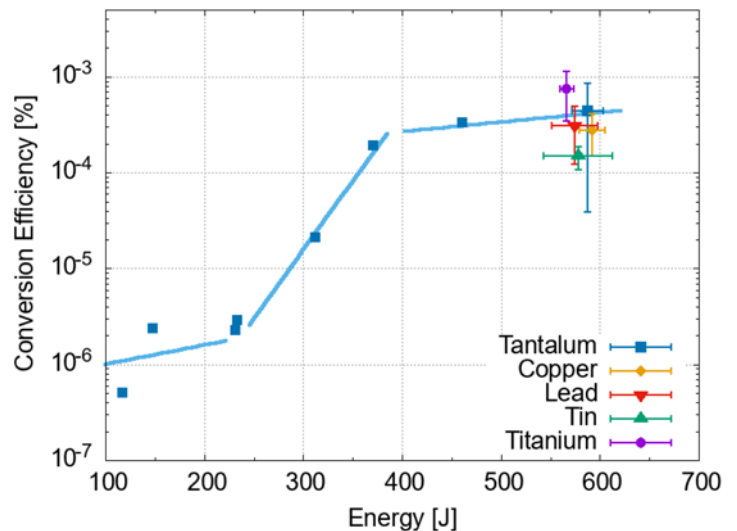


Figure 11. The profile of conversion efficiency from laser energy to electron kinetic energy as a function of incident laser energy. The colour code in the legend represents different target materials having similar thickness range, i.e. $\approx 10 \mu\text{m}$. The data of different target materials are compared with published result of the tantalum target (see Figure 10 of the reference by Singh *et al.*, (Ref. 24)).

varies between Beg and ponderomotive scalings (Ref. 34), however; electron temperature is in accordance with Beg scaling (Ref. 39) at high intensities, i.e. $>10^{16} \text{ W cm}^{-2}$ (see Figure 2). Moreover, Beg scaling is observed in long plasma scale length ($\sim 100 \mu\text{m}$); however, ponderomotive scaling is usually valid for small plasma scale lengths where laser pulse is tightly focused. In addition, the electron temperature scaling is bit different from the one that corresponds to the suprathermal one (Ref. 37), however, Beg dependence is in consistent with the extended Gibbons model (Ref. 29). For the given experimental conditions, a positive correlation is observed between the electrons following the Beg scaling (Ref. 29) and maximum energy of accelerated ions (Ref. 44), however; identifying the physical mechanism is bit difficult due to presence of the different instabilities under mentioned intensity range of the experiment.

Apart from characteristics of the electron temperature scaling and fluctuations in electron parameters, the step like behaviour in the profile of conversion efficiency from laser energy to hot electrons (see Figure 11) indicates the specific non-linearity that

can be attributed to experimental conditions and plasma parameters. At laser intensity of $\sim 10^{16} \text{ W cm}^{-2}$, LPI is dominated by parametric instabilities (SRS, TPD) which can be responsible for non-collisional absorption and generate large fluxes of hot electrons. Cristoforetti *et al.* investigated the extent and time history of SRS and TPD instabilities, driven by the interaction of PALS laser at an intensity $\sim 1.2 \times 10^{16} \text{ W cm}^{-2}$ with plasma scalelength $\sim 100 \mu\text{m}$ produced from irradiation of a flat plastic target (Ref. 43). Moreover, Cristoforetti *et al.* measured the hot electron energy in the range of 40–50 keV which is in close agreement with the electron temperature of our measurements. In addition, the self-focusing of the laser beam in the plasma can be produced by a relativistic mechanism (Ref. 45). The relativistic nonlinearity should appear immediately when the power of the incident laser exceeds the threshold required for self-focusing ($P_{cr} = 17.4 n_{cr}/n_e$) in GW (Ref. 46), where n_{cr} and n_e are the critical density and measured value of plasma density, respectively.

Furthermore, at the lower intensity case ($\leq 10^{16} \text{ W cm}^{-2}$), self-focusing does not occur because the power could barely reach the

critical power of relativistic self-focusing (P_{cr}). However, the measured data from femtosecond interferometry shows that electron plasma density $n_e \approx 3 \times 10^{19} \text{ W cm}^{-2}$ of the scale length $\approx 100 \mu\text{m}$, can be produced on the front surface of the irradiated target, 100 ps before the maximum laser power (Ref. 23). For the laser wavelength $1.315 \mu\text{m}$, the required $P_{cr} \approx 0.45 \text{ TW}$ is less than the 1.5 TW used in this experiment which implies that for laser energy $\geq 250 \text{ J}$ and intensity $\geq 8 \times 10^{15} \text{ W cm}^{-2}$, the possibility of self-focusing cannot be ignored along with other nonlinear effects (Ref. 24). In the given experimental scenarios, plasma density must be sufficiently thick to allow the creation of a self-focusing channel and the threshold intensity for both the ponderomotive and relativistic filamentation which is reachable during the LPI. Moreover, the nonlinear characteristic in the profile of conversion efficiency can be seen at energy threshold $\sim 250 \text{ J}$ (see Figure 11) which is in closer agreement with our analogy and hypothesis. Figure 11 clearly shows that the relativistic self-focusing is not emerging significantly for laser energies $\leq 250 \text{ J}$, however; for given laser and plasma parameters, it can occur at higher laser energies ($\geq 250 \text{ J}$).

Conclusion

This paper presents basic results of an experiment in which a sub-nanosecond pulse ($\sim 350 \text{ ps}$) from an iodine laser was focused on metal foil targets having different atomic numbers (Cu, Ta, Ti, Sn, Pb) for laser intensities between $\sim 10^{15}$ and $\sim 3 \times 10^{16} \text{ W cm}^{-2}$. The hot electrons were characterized by measuring the energy spectrum using array of electron spectrometers for different thickness of foil targets in the range of $1\text{--}100 \mu\text{m}$. The measured electron temperature is observed in the range between 30 and 80 keV for the given range of laser intensities. The temperature scaling of different targets is also compared with experimental and simulation results from sub-nanosecond, sub-picosecond and multi-picosecond laser systems. In this experimental condition, the electron temperature scaling varies in between Beg and ponderomotive scalings. Moreover, we also observed that conversion efficiency from laser energy to hot electrons is showing step-like behaviour and it varies nonlinearly with increasing laser energy in the range between $\sim 10^{-6}$ and $\sim 10^{-3}$ for laser energy in the range between 100 and 600 J , respectively. For the given plasma parameters, the nonlinear profile of conversion efficiency which has step-like behaviour can be attributed to either or combined effects of parametric instabilities, self-focusing and relativistic filamentation. The experimental results associated with conversion efficiency and temperature scaling for different foil targets are not only important for the understanding of hot electron generation in long-pulse, high-intensity laser–solid interaction experiments, but also crucial for the experiments relevant to fast-ignition (Ref. 47), laboratory astrophysics (Ref. 48, 49) and high energy density science (Ref. 50).

Data availability statement. The data generated and/or analyzed during the current study are not publicly available for legal/ethical reasons but are available from the corresponding author on reasonable request. The data that support the findings of this study are available from the corresponding author upon reasonable request.

Acknowledgements. The research presented in this paper was supported by the Access to the PALS RI under the Laserlab-Europe V project (Grant Agreement No. 871124), by the Czech Republic's Ministry of Education, Youth and Sports – the projects: Prague Asterix Laser System (LM2023068) and Creating and probing dense plasmas at the PALS facility (CZ.02.1.01/0.0/0.0/16013/0001552). The research leading to these results has received funding from the Czech Science Foundation (Grant No. 23-05027M

and 19-24619S). The support of CTU student support project 'Research on optical (nano) structures and laser plasma' SGS19/192/OHK4/3T/14 is gratefully acknowledged as well as the support by the international project called 'PMW', co-financed by the Polish Ministry of Science and Higher Education within the framework of the scientific financial resources for 2021–2022 under the Contract No. 5084/PALS/2020/0 (Project No. PALS002628). This scientific work is also supported by the project Advanced research using high intensity laser produced photons and particles (ADONIS) CZ.02.1.01/0.0/0.0/16019/0000789 from European Regional Development Fund (ERDF) as well as supported by EUROfusion Consortium, funded by the European Union via the Euratom Research and Training Programme (Grant Agreement No. 101052200-EUROfusion).

References

- Láska L, Jungwirth K, Krása J, Pfeifer M, Rohlena K, Ullschmied J, Badziak J, Parys P, Wolowski J, Gammino S, Torrisi L and Boody FP (2005) Charge-state and energy enhancement of laser-produced ions due to nonlinear processes in preformed plasma. *Applied Physics Letters* **86**, 081502.
- Gitomer SJ, Jones RD, Begay F, Ehler AW, Kephart JF and Kristal R (1986) Fast ions and hot electrons in the laser–plasma interaction. *The Physics of Fluids* **29**, 2679–2688.
- Singh PK, Cui Y, Adak A, Lad AD, Chatterjee G, Brijesh P, Sheng Z and Kumar GR (2015) Contrasting levels of absorption of intense femtosecond laser pulses by solids. *Scientific Reports* **5**, 1–7
- Zylstra A, Hurricane O, Callahan D, Kritcher A, Ralph J, Robey H, Ross J, Young C, Baker K, Casey D, Doppner T, Divol L, Hohenberger M, Pape S, Pak A, Patel P, Tommasini R, Ali S, Amendt P, Atherton L, Bachmann B, Bailey D, Benedetti L, Hopkins L, Betti R, Bhandarkar S, Biener J, Bionta R, Birge N, Bond E, Bradley D, Braun T, Briggs T, Bruhn M, Celliers P, Chang B, Chapman T, Chen H, Choate C, Christopherson A, Clark D, Crippen J, Dewald E, Dittrich T, Edwards M, Farmer W, Field J, Fittinghoff D, Frenje J, Gaffney J, Johnson M, Glenzer S, Grim G, Haan S, Hahn K, Hall G, Hammel B, Harte J, Hartouni E, Heebner J, Hernandez V, Herrmann H, Herrmann M, Hinkel D, Ho D, Holder J, Hsing W, Huang H, Humbird K, Izumi N, Jarrott L, Jeet J, Jones O, Kerbel G, Kerr S, Khan S, Kilkenny J, Kim Y, Kleinrath H, Kleinrath V, Kong C, Koning J, Kroll J, Kruse M, Kustowski B, Landen O, Langer S, Larson D, Lemos N, Lindl J, Ma T, MacDonald M, MacGowan B, Mackinnon A, MacLaren S, MacPhee A, Marinak M, Mariscal D, Marley E, Masse L, Meaney K, Meezan N, Michel P, Millot M, Milovich J, Moody J, Moore A, Morton J, Murphy T, Newman K, Nicola J, Nikroo A, Nora R, Patel M, Pelz L, Peterson J, Ping Y, Pollock B, Ratledge M, Rice N, Rinderknecht H, Rosen M, Rubery M, Salmonson J, Sater J, Schiaffino S, Schlossberg D, Schneider M, Schroeder C, Scott H, Sepke S, Sequoia K, Sherlock M, Shin S, Smalyuk V, Spears B, Springer P, Stadermann M, Stoupin S, Strozzzi D, Suter L, Thomas C, Town R, Tubman E, Troselle C, Volegov P, Weber C, Widmann K, Wild C, Wilde C, Wonterghem B, Woods D, Woodworth B, Yamaguchi M, Yang S and Zimmerman GI (2022) Burning plasma achieved in inertial fusion. *Nature* **601**, 542–548.
- Kritcher A, Young C, Robey H, Weber C, Zylstra A, Hurricane O, Callahan D, Ralph J, Ross J, Baker K, Casey D, Clark D, Doppner T, Divol L, Hohenberger M, Berzak Hopkins L, Le Pape S, Meezan N, Pak A, Patel P, Tommasini R, Ali S, Amendt P, Atherton L, Bachmann B, Bailey D, Benedetti L, Betti R, Bhandarkar S, Biener J, Bionta R, Birge N, Bond E, Bradley D, Braun T, Briggs T, Bruhn M, Celliers P, Chang B, Chapman T, Chen H, Choate C, Christopherson A, Crippen J, Dewald E, Dittrich T, Edwards M, Farmer W, Field J, Fittinghoff D, Frenje J, Gaffney J, Gatun Johnson M, Glenzer S, Grim G, Haan S, Hahn K, Hall G, Hammel B, Harte J, Hartouni E, Heebner J, Hernandez V, Herrmann H, Herrmann M, Hinkel D, Ho D, Holder J, Hsing W, Huang H, Humbird K, Izumi N, Jarrott L, Jeet J, Jones O, Kerbel G, Kerr S, Khan S, Kilkenny J, Kim Y, Geppert-Kleinrath H, Geppert-Kleinrath V, Kong C, Koning J, Kruse M, Kroll J, Kustowski B, Landen O, Langer S, Larson D, Lemos N, Lindl J, Ma T, MacDonald M,

- MacGowan B, Mackinnon A, MacLaren S, MacPhee A, Marinak M, Mariscal D, Marley E, Masse L, Meaney K, Michel P, Millot M, Milovich J, Moody J, Moore A, Morton J, Murphy T, Newman K, Nicola J, Nikroo A, Nora R, Patel M, Pelz L, Peterson J, Ping Y, Pollock B, Ratledge M, Rice N, Rinderknecht H, Rosen M, Rubery M, Salmonson J, Sater J, Schiaffino S, Schlossberg D, Schneider M, Schroeder C, Scott H, Sepke S, Sequoia K, Sherlock M, Shin S, Smalyuk V, Spears B, Springer P, Stadermann M, Stoupin S, Strozzio D, Suter L, Thomas C, Town R, Trosseille C, Tubman E, Volegov P, Widmann K, Wild C, Wilde C, Wouterghem B, Woods D, Woodworth B, Yamaguchi M, Yang S and Zimmerman G (2022) Design of inertial fusion implosions reaching the burning plasma regime. *Nature Physics* **18**, 251–258.
6. Pisarczyk T, Renner O, Dudzak R, Chodukowski T, Rusiniak Z, Domanski J, Badziak J, Dostal J, Krupka M, Singh S, Klir D, Ehret M, Gajdos P, Szydłowska A, Rosinski M, Tchórz P, Szymanski M, Krasa J, Burian T, Pfeifer M, Cikhartd J, Jelinek S, Kocourkova G, Batani D, Batani K, Santos J, Vlachos C, Ospina-Bohórquez V, Volpe L, Borodziuk S, Krus M and Juha L (2022) Influence of the magnetic field on properties of hot electron emission from ablative plasma produced at laser irradiation of a disc-coil target. *Plasma Physics and Controlled Fusion* **64**, 115012.
 7. Pisarczyk T, Gus'kov S, Chodukowski T, Dudzak R, Korneev P, Demchenko N, Kalinowska Z, Dostal J, Zaras-Szydłowska A, Borodziuk S, Juha L, Cikhartd J, Krasa J, Klir D, Cikhartdova B, Kubes P, Krousky E, Krus M, Ullschmied J, Jungwirth K, Hrebicek J, Medrik T, Golasowski J, Pfeifer M, Renner O, Singh S, Kar S, Ahmed H, Skala J and Pisarczyk P (2017) Kinetic magnetization by fast electrons in laser-produced plasmas at sub-relativistic intensities. *Physics of Plasmas* **24**, 102711.
 8. Antici P, Albertazzi B, Audebert P, Buffecheux S, Hannachi F, d'Humières E, Gobet F, Grismayer T, Mancic A, Nakatsutsumi M, Plaisir C, Romagnani L, Tarisien M, Pépin H, Sentoku Y and Fuchs J (2012) Measuring hot electron distributions in intense laser interaction with dense matter. *New Journal of Physics* **14**, 063023.
 9. Pisarczyk T, Gus'kov S, Zaras-Szydłowska A, Dudzak R, Renner O, Chodukowski T, Dostal J, Rusiniak Z, Burian T, Borisenko N, Rosinski M, Krupka M, Parys P, Klir D, Cikhartd J, Rezac K, Krasa J, Rhee Y-J, Kubes P, Singh S, Borodziuk S, Krus M, Juha L, Jungwirth K, Hrebicek J, Medrik T, Golasowski J, Pfeifer M, Skala J, Pisarczyk P and Korneev PH (2018) Magnetized plasma implosion in a snail target driven by a moderate-intensity laser pulse. *Scientific Reports* **8**, 1–11.
 10. Forslund D, Kindel J and Lee K (1977) Theory of hot-electron spectra at high laser intensity. *Physical Review Letters* **39**, 284.
 11. Brunel F (1987) Not-so-resonant, resonant absorption. *Physical Review Letters* **59**, 52.
 12. Mangles SPD, Walton BR, Tzoufras M, Najmudin Z, Clarke RJ, Dangor AE, Evans R, Fritzler S, Gopal A, Hernandez-Gomez C, Mori WB, Rozmus W, Tatarakis M, Thomas AGR, Tsung FS, Wei MS, Krushelnick K (2005) Electron Acceleration in Cavitated Channels Formed by a Petawatt Laser in Low-Density Plasma. *Physical Review Letters* **94**, 245001.
 13. Malka V, Fritzler S, Lefebvre E, Aleanard MM, Burgy F, Chambaret JP, Chemin JF, Krushelnick K, Malka G, Mangles S, Najmudin Z, Pittman M, Rousseau J-P, Scheurer J-N, Walton B and Dangor A (2002) Electron acceleration by a wake field forced by an intense ultrashort laser pulse. *Science* **298**, 1596–1600
 14. Tajima T and Dawson JM (1979) Laser electron accelerator. *Physical Review Letters* **43**, 267.
 15. Ridgers C, Brady CS, Ducloux R, Kirk J, Bennett K, Arber T, Robinson A and Bell A (2012) Dense electron-positron plasmas and ultraintense Γ rays from laser-irradiated solids. *Physical Review Letters* **108**, 165006.
 16. Ta Phuoc K, Corde S, Thauray C, Malka V, Tafzi A, Goddet JP, Shah R, Sebban S and Rousse A (2012) All-optical Compton gamma-ray source. *Nature Photonics* **6**, 308–311
 17. Singh S, Armstrong CD, Kang N, Ren L, Liu H, Hua N, Rusby DR, Klimo O, Versaci R, Zhang Y, Sun M, Zhu B, Lei A, Ouyang X, Lancia L, Garcia A, Wagner A, Cowan T, Zhu J, Schlegel T, Weber S, McKenna P, Neely D, Tikhonchuk V and Kumar D (2021) Bremsstrahlung emission and plasma characterization driven by moderately relativistic laser–plasma interactions. *Plasma Physics and Controlled Fusion* **63**, 035004.
 18. Glinec Y, Faure J, Le Dain L, Darbon S, Hosokai T, Santos J, Lefebvre E, Rousseau JP, Burgy F, Mercier B and Malka V (2005) High-resolution Γ -ray radiography produced by a laser-plasma driven electron source. *Physical Review Letters* **94**, 025003.
 19. Cowan T, Hunt A, Phillips T, Wilks S, Perry M, Brown C, Fountain W, Hatchett S, Johnson J, Key M, Parnell T, Pennington D, Snavely R and Takahashi Y (2000) Photonuclear fission from high energy electrons from ultraintense laser–solid interactions. *Physical Review Letters* **84**, 903.
 20. Singh S, Versaci R, Laso Garcia A, Morejon L, Ferrari A, Molodtsova M, Schwengner R, Kumar D and Cowan T (2018) Compact high energy x-ray spectrometer based on forward Compton scattering for high intensity laser plasma experiments. **89**, 085118.
 21. Cui YQ, Wang WM, Sheng ZM, Li YT and Zhang J (2013) Laser absorption and hot electron temperature scalings in laser–plasma interactions. *Plasma Physics and Controlled Fusion* **55**, 085008.
 22. Krupka M, Singh S, Pisarczyk T, Dostal J, Kalal M, Krasa J, Dudzak R, Burian T, Jelinek S, Chodukowski T, Rusiniak Z, Krus M and Juha L (2021) Design of modular multi-channel electron spectrometers for application in laser matter interaction experiments at Prague Asterix Laser System. *Review of Scientific Instruments* **92**, 023514.
 23. Pisarczyk T, Kalal M, Gus'kov S, Batani D, Renner O, Santos J, Dudzak R, Zaras-Szydłowska A, Chodukowski T, Rusiniak Z, Dostal J, Krasa J, Krupka M, Kochetkov L, Singh S, Cikhartd J, Burian T, Krus M, Pfeifer M, Cristoforetti G, Gizzi L, Baffigi F, Antonelli L, Demchenko N, Rosinski M, Terwinska D, Borodziuk S, Kubes P, Ehret M, Juha L, Skala J and Korneev Ph (2020) Hot electron retention in laser plasma created under terawatt subnanosecond irradiation of Cu targets. *Plasma Physics and Controlled Fusion* **62**, 115020.
 24. Singh S, Krupka M, Istoksaika V, Krasa J, Giuffrida L, Dudzak R, Dostal J, Burian T, Versaci R, Margarone D, Pisarczyk T, Krus M and Juha L (2022) Hot electron and x-ray generation by sub-ns kJ-class laser-produced tantalum plasma. *Plasma Physics and Controlled Fusion* **64**, 105012.
 25. Galy J, Maučec M, Hamilton D, Edwards R and Magill J (2007) Bremsstrahlung production with high-intensity laser matter interactions and applications. *New Journal of Physics* **9**, 23.
 26. Rusby DR, Cochran GE, Aghedo A, Albert F, Armstrong CD, Haid A, Kemp AJ, Kerr SM, King PM, Lemos N, Manuel MJE, Ma T, MacPhee AG, Pagano I, Pak A, Scott GG, Siders CW, Simpson RA, Sinclair M, Wilks SC, Williams GJ and Mackinnon AJ (2023) Enhanced electron acceleration by high-intensity lasers in extended (confined) pre-plasma in cone targets. *Physics of Plasmas* **30**, 023103.
 27. Jungwirth K, Cejnarova A, Juha L, Kralikova B, Krasa J, Krousky E, Krupickova P, Laska L, Masek K, Mocek T, Pfeifer M, Präg A, Renner O, Rohlena K, Rus B, Skala J, Straka P and Ullschmied J (2001) The Prague asterix laser system. *Physics of Plasmas* **8**, 2495–2501.
 28. Singh S, Slavicek T, Hodak R, Versaci R, Pridal P and Kumar D (2017) Absolute calibration of imaging plate detectors for electron kinetic energies between 150 keV and 1.75 MeV. *Review of Scientific Instruments* **88**, 075105.
 29. Beg F, Bell A, Dangor A, Danson C, Fewes A, Glinsky M, Hammel B, Lee P, Norreys P and Tatarakis M (1997) A study of picosecond laser–solid interactions up to 1019 W cm^{-2} . *Physics of Plasmas* **4**, 447–457
 30. Wilks SC, Kruer WL, Tabak M and Langdon AB (1992) Absorption of ultra-intense laser pulses. *Physical Review Letters* **69**(9) 1383–1386.
 31. Pukhov A, Sheng ZM and Meyer-ter Vehn J (1999) Particle acceleration in relativistic laser channels. *Physics of Plasmas* **6**, 2847–2854.
 32. Yu J, Jiang Z, Kieffer JC and Krol A (1999) Hard x-ray emission in high intensity femtosecond laser–target interaction. *Physics of Plasmas* **6**, 1318–1322.
 33. Haines MG, Wei MS, Beg FN and Stephens RB (2009) Hot-electron temperature and laser-light absorption in fast ignition. *Physical Review Letters* **102**(4) 045008.
 34. Kluge T, Cowan T, Debus A, Schramm U, Zeil K and Bussmann M (2011) Electron temperature scaling in laser interaction with solids. *Physical Review Letters* **107**, 205003.

35. Chen H, Link A, Sentoku Y, Audebert P, Fiuza F, Hazi A, Heeter RF, Hill M, Hobbs L, Kemp AJ, Kemp GE, Kerr S, Meyerhofer DD, Myatt J, Nagel SR, Park J, Tommasini R and Williams GJ (2015) The scaling of electron and positron generation in intense laser–solid interactions. *Physics of Plasmas* **22**, 056705.
36. Simpson RA, Scott GG, Mariscal D, Rusby D, King PM, Grace E, Aghedo A, Pagano I, Sinclair M, Armstrong C, Manuel MJE, Haid A, Flippo K, Winslow L, Gatu-Johnson M, Frenje JA, Neely D, Kerr S, Williams GJ, Andrews S, Cauble R, Charron K, Costa R, Fischer B, Maricle S, Stuart B, Albert F, Lemos N, Mackinnon A, MacPhee A, Pak A and Ma T (2021) Scaling of laser-driven electron and proton acceleration as a function of laser pulse duration, energy, and intensity in the multi-picosecond regime. *Physics of Plasmas* **28**, 013108.
37. Gibbon P and Bell A (1992) Collisionless absorption in sharp-edged plasmas. *Physical Review Letters* **68**, 1535.
38. Gibbon P (2012) Physics of high-intensity laser-plasma interactions. *La Rivista del Nuovo Cimento* **35**, 1826–9850.
39. Kluge T, Bussmann M, Schramm U and Cowan TE (2018) Simple scaling equations for electron spectra, currents, and bulk heating in ultra-intense short-pulse laser–solid interaction. *Physics of Plasmas* **25**, 073106.
40. Quinn MN, Yuan XH, Lin XX, Carroll DC, Tresca O, Gray RJ, Coury M, Li C, Li YT, Brenner CM, Robinson APL, Neely D, Zielbauer B, Aurand B, Fils J, Kuehl T and McKenna P (2011) Refluxing of fast electrons in solid targets irradiated by intense, picosecond laser pulses. *Plasma Physics and Controlled Fusion* **53**, 025007.
41. Berger MJ, Coursey JS and Zucker MA (1999) ESTAR, PSTAR, and ASTAR: Computer programs for calculating stopping-power and range tables for electrons, protons, and helium ions (version 2.0.1) <http://physics.nist.gov/Star> (accessed 15 March 2024).
42. Montgomery DS (2016) Two decades of progress in understanding and control of laser plasma instabilities in indirect drive inertial fusion. *Physics of Plasmas* **23**.
43. Cristoforetti G, Antonelli L, Mancelli D, Atzeni S, Baffigi F, Barbato F, Batani D, Boutoux G, D'Amato F, Dostal J, Dudzak R, Filippov E, Gu Y, Juha L, Klimo O, Krus M, Malko S, Martynenko A, Nicolai Ph, Ospina V, Pikuz S, Renner O, Santos J, Tikhonchuk V, Trela J, Viciani S, Volpe L, Weber S and Gizzi L (2019) Time evolution of stimulated Raman scattering and two-plasmon decay at laser intensities relevant for shock ignition in a hot plasma. *High Power Laser Science and Engineering* **7**, e51.
44. Krasa J, Klir D, Rezac K, Cikhart J, Krus M, Velyhan A, Pfeifer M, Buryskova S, Dostal J, Burian T, Dudzak R, Turek K, Pisarczyk T, Kalinowska Z, Chodukowski T and Kaufman J (2018) Production of relativistic electrons, MeV deuterons and protons by sub-nanosecond terawatt laser. *Physics of Plasmas* **25**, 113112.
45. Sun GZ, Ott E, Lee Y and Guzdar P (1987) Self-focusing of short intense pulses in plasmas. *The Physics of fluids* **30**, 526–532.
46. Habara H, Adumi K, Yabuuchi T, Nakamura T, Chen Z, Kashihara M, Kodama R, Kondo K, Kumar G, Lei L, Matsuoka T, Mima K and Tanaka K (2006) Surface acceleration of fast electrons with relativistic self-focusing in preformed plasma. *Physical Review Letters* **97**, 095004.
47. Klimo O, Psikal J, Tikhonchuk VT and Weber S (2014) Two-dimensional simulations of laser–plasma interaction and hot electron generation in the context of shock-ignition research. *Plasma Physics and Controlled Fusion* **56**, 055010.
48. Kumar D, Singh S, Ahmed H, Dudžák R, Dostál J, Chodukowski T, Giuffrida L, Hadjisolomu P, Hodge T, Juha L, Krouský E, Krüs M, Li Y, Lutoslawski P, Marco MD, Pfeifer M, Rusiniak Z, Skála J, Ullschmeid J, Pisarczyk T, Borghesi M and Kar S (2020) Magnetic field generation using single-plate targets driven by kJ-ns class laser. *Plasma Physics and Controlled Fusion* **62**, 125024.
49. Sanyasi AK, Awasthi LM, Mattoo SK, Srivastava PK, Singh SK, Singh R and Kaw PK (2013) *Physics of Plasmas* **20**, 122113.
50. Weber S, Bechet S, Borneis S, Brabec L, Bučka M, Chacon-Golcher E, Ciappina M, DeMarco M, Fajstavr A, Falk K, Garcia ER, Grosz J, Gu YJ, Hernandez JC, Holec M, Janečka P, Jantač M, Jirka M, Kadlecova H, Khikhlukha D, Klimo O, Korn G, Kramer D, Kumar D, Lastovička T, Lutoslawski P, Morejon L, Olšovcová V, Rajdl M, Renner O, Rus B, Singh S, Šmid M, Sokol M, Versaci R, Vrána R, Vranic M, Vyskočil J, Wolf A and Yu Q (2017) P3: An installation for high-energy density plasma physics and ultra-high intensity laser–matter interaction at ELI-Beamlines. *Matter and Radiation at Extremes* **2**, 149–176.